Accepted Manuscript

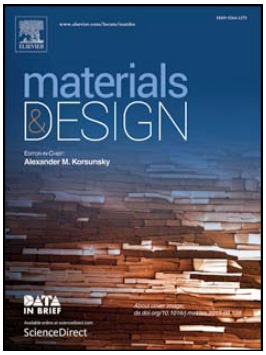

Analysis and modelling of mechanical anchorage of 4D/5D hooked end steel fibres

Sadoon Abdallah, Mizi Fan, David W.A. Rees

PII: S0264-1275(16)31291-6
DOI: doi: 10.1016/j.matdes.2016.09.107
Reference: JMADE 2357

To appear in:

Received date: 4 July 2016
Revised date: 20 September 2016
Accepted date: 30 September 2016

Please cite this article as: Sadoon Abdallah, Mizi Fan, David W.A. Rees, Analysis and modelling of mechanical anchorage of 4D/5D hooked end steel fibres, (2016), doi: 10.1016/j.matdes.2016.09.107

Analysis and modelling of mechanical anchorage of 4D/5D hooked end steel fibres

Sadoon Abdallah, Mizi Fan* and David W.A. Rees

College of Engineering, Design and Physical Sciences, Brunel University
Uxbridge, UB8 3PH, London, United Kingdom

Abstract

This paper represents an analytical model to predict the influence of the fibre geometry on the pull-out behaviour of various geometrical hooked end steel fibres. The model is established based on the concept of a frictional pulley along with two, three and four plastic hinges to simulate the mechanical anchorage effect provided by the hook. The mechanical contribution of the hook is a function of the cold work needed to straighten the fibre during the pull-out. The input parameters used in this model are directly related to geometrical and mechanical properties of each fibre. Model predictions are validated against experimental results for single fibre pull-out tests, and very good agreement is shown.

Keywords:

Pull-out behaviour
Ultra-high performance mortar
Anchorage effect
Hook geometry
Plastic hinge

**Corresponding author: Professor, Head of Research, Email: mizi.fan@brunel.ac.uk, Tel.: +44 189 5266466*

1. Introduction

Brittle materials such as concrete and mortar are well known for their low ability to resist tensile stresses and crack propagation [1,2]. The incorporation of randomly distributed steel fibres to a cementitious matrix could significantly improve their tensile behaviour, ductility, impact resistance and crack resistance [3-7].

The fibre contribution is mainly reflected when the concrete cracking initiates and often enhances the post-cracking behaviour due to the improved stress transfer provided by the fibre bridging of the cracked sections [8]. The efficiency of fibre in transferring stress is greatly dependent on bond mechanisms between fibre and matrix [9]. Therefore, the knowledge of the bond mechanisms is a key factor to understand the tensile behaviour of steel fibre-reinforced concrete (SFRC), especially for hooked end fibres. The bond characteristics are commonly assessed using the single fibre pull-out test, which is able to determine the interfacial properties between the fibre and the surrounding cementitious matrix [10,11]. A review of the literature indicated that pull-out tests have mostly been performed by means of a single-fibre on single-sided test due to the simplicity and reliability of the test [12]. On the other hand, a pull-out test on a multiple-fibre specimen is more complex to manufacture and difficult to test [13]. Moreover, use of these tests to measure pull-out behaviour quantitatively is complicated by the difficulty in achieving a uniform distribution of load to all the fibres [14].

Numerous experimental and analytical investigations have been conducted to determine the bond mechanisms between steel fibre and matrix [8,15-17]. Based on the results, it is concluded that the mechanical deformation of fibres and matrix strength play a major role on pull-out response. However, there have been few attempts to model the effect of fibre geometry on the pull-out behaviour of steel fibres. The first predictions of the pull-out force of hooked end fibres were proposed by Alwan et al. [18] and Chanvillard [19]. Alwan et al. [18] developed an analytical model to predict the mechanical anchorage contribution provided by the fibre hook. Their model is based on the concept of a frictional pulley along with two plastic hinges. The mechanical contribution provided by the fibre is considered as a function of the cold work needed to straighten the hook during

pull-out. To predict the entire pull-out versus slip response a two-step process is required corresponding to (i) the contribution of the two hinges, and (ii) the superposition of the frictional and mechanical components. An alternative approach was proposed by Chanvillard [19] using principles of virtual work dividing the hook into distinct curved and straight parts.

Sujivorakul et al. [20] extended the straight fibre pull-out model developed by Naaman et al. [21] by adding a non-linear spring at the end of the fibre to simulate the mechanical anchorage contribution. In later work Laranjeira et al. [22], Ghoddousi et al. [23], and Lee et al. [12] proposed new models which are quite comparable to the model developed by Alwan et al. [18]. Soetens et al. [24] have proposed a semi-analytical model to predict the pull-out behaviour of hooked end steel fibres based on the principle of virtual work developed by Chanvillard [19]. Zile et al. [25] have developed an analytical model to simulate the mechanical contribution of fibre geometry to the pull-out response of crimped and hooked end steel fibres. This model is based both on the amount of plastic work required to straighten the fibre during pull-out and friction in the curved ducts. Won et al. [26] have developed an analytical model based on model developed by Zile et al.[25] to simulate bond mechanism of arch-type steel fibres. The friction model is more convenient to adopt the recent designs, where 4D and 5D hooked end steel fibres of improved shape were introduced. These fibres were designed to achieve high levels of fibre anchoring, tensile strength and ductility. Although fibre-matrix bond mechanisms of old generation of hooked end fibres (named 3D) have been largely investigated, the existing models are not sufficient to predict the pull-out behaviour of newly fibres (i.e. 4D and 5D). This is because the mechanisms associated with pull-out behaviour of these new hooked end fibres (i.e. 4D and 5D) are not yet understood. The main objective of this research is to develop a simple analytical model to simulate the mechanical anchorage contribution provided by the hook of 4D and 5D fibres. The proposed model extends the frictional pulley model developed by Alwan et al. [18] to include fibres with three and four plastic hinges in their end hooks. The input parameters of the model are the geometrical and mechanical properties of various hooked end fibres. It should be noted that the model is validated against experimental pull-out test results of all fibres embedded in ultra-high performance mortar (UHPM) only. According to experimental

observations by the authors [27], the hook of 4D and 5D fibres was found to be only partially deformed and straightened when embedded in medium strength matrix.

2. Experimental program

2.1. Materials and specimens

The mix proportions of the ultra-high performance mortar (UHPM) adopted in this study is summarized in Table 1. Three types of commercially available Dramix hooked end steel fibres (H), namely 3DH, 4DH and 5DH were used in the pull-out tests (Table 2). These fibres have a same length (60 mm), diameter (0.9 mm) and aspect ratio (l/d = 65) and only differ in the hook geometry and tensile strength. The geometrical properties of hooked end fibres are depicted in Fig. 1 and detailed in Table 2. To determine the fibre/matrix interface characteristics, straight fibres (S) (i.e. 3DS, 4DS, and 5DS) were also tested. The straight fibres were prepared by cutting off the hooked ends of the 3DH, 4DH and 5DH fibres.

The pull-out tests on single steel fibres were performed using cylinders with a diameter of 100 mm and height of 50 mm (Fig. 2). In each test specimen, a single steel fibre was carefully placed through a hole in the bottom of each mould. The embedded length (l_E) was one half of the overall fibre length (i.e. 30 mm). For compressive strength tests, three cubes (100 × 100 × 100 mm) were also prepared. During preparation, the dry components were firstly mixed for approximately 1 minute before water and the superplasticizer were added. This was then mixed for 11 minutes, a period which experience has shown is appropriate to result in a homogenous mixture. After casting and vibration, the specimens were covered with a thin polyethylene film to avoid retaining the escaping moisture and left for 24 hours at room temperature. The specimens were then removed from moulds and cured for a further 28 days in the conditioning chamber, where the temperature was held at 20 ± 2°C and the relative humidity at 96 ± 4 %. All specimens were tested at an age of 30 ± 2 days and the average value of three specimens was adopted, both for the compressive strength and pull-out tests.

2.2. Pull-out test

The pull-out tests were performed using a specially designed grip system, as illustrated in Fig. 2, which was attached to an Instron 5584 universal testing machine. The grips were designed such that the forces applied to the fibre provided a true reflection of the real situation experienced by fibres bridging a crack. The body of the gripping system was machined in a lathe using mild steel and had a tapered end to allow the insertion of four M4 grub screws (Fig. 2). These were then tightened around the steel fibre to an equal torque for an even distribution of gripping pressure to minimise the deformation of the fibre ends and avoid breakage at the tip. Two linear variable differential transformer (LVDT) transducers were used to measure the distance travelled by the steel fibre relative to the concrete face during testing (i.e. the pull-out distance). They were held in place using aluminium sleeves on either side of the main grip body (Fig. 2). The LVDT's had ball bearings at the tips to allow for accurate readings on the face of the samples. The sample was secured to the Instron base using clamps with riser blocks and M16 studs. The specimen was positioned on a brass round disc to remove any discrepancies in the sample base and allow for distortion. In all pull-out tests, a displacement rate of 10 µm/s was adopted.

2.3. Experimental results

The average load-slip curves obtained from pull-out test of straight fibres (3DS, 4DS and 5DS) are presented in Fig. 3. It can be seen that the pull-out behaviour of the straight fibres mainly characterized by a rapid increase followed by a sudden drop in pull-out load, indicating that the full fibre debonding. Afterwards, the pull-out load continues to decrease with an increase in the slip. All straight fibres have approximately the same value of the maximum pull-out load, as expected. However, there is a remarkable difference in post peak behaviour of each fibres type. Some of this difference may be a result of the deformation of the fibre end owing to the cutting process which provides some mechanical anchorage, leading to increase the pull-out resistance. This can alter the frictional coefficient produced by a 'ploughing' effect. Similar behaviour has been observed by Wille and Naaman [28]

Pull-out behaviour of hooked end steel fibres (3DH, 4DH and 5DH) is shown in Fig. 4. It can be observed that overall the hook geometry has a significant influence on the pull-out response. The high anchorage effect provided by the lengthy hook of 4DH and 5DH

fibres enhances the pull-out behaviour significantly, generating higher pull-out load and pull-out work as compared to 3DH fibre. The full deformation and straightening of fibre hook without matrix damage have been observed for all fibres. The coefficient of variation (CoV) of the average P_{max} (three tests in each series) indicates the consistency of the test results with the CoV values lying below 4% for both straight and hooked end steel fibres.

3. Mathematical equations for fibre pull-out behaviour

It has been shown from experimental observations that the pull-out process of a hooked end steel fibre is quite similar to that of a straight fibre up to fibre complete debonding. After this, the mechanical anchorage effect provided by the hook is mainly responsible for the pull-out resistance. The mathematical derivation of pull-out behaviour of a straight fibre has been explained in detail in Naaman et al. [21]. The pull-out process of hooked end fibre can be divided into three different stages as follows (Figs. 5a-d):

3.1. Elastic and partial debonding stage

When $P \leq P_1$ (Fig. 6), a part of the fibre is debonded from the matrix while the remaining part is still fully bonded to the matrix. Here, a part of the pull-out force is resisted partially by elastic shear stresses, while the other part is resisted partially by interfacial frictional stresses (Fig. 5a). In that stage, the pull-out load (P) and the corresponding slip (Δ) are given as [21]:

$$P = \tau_f \psi u + \frac{\tau_{max}}{\lambda} \frac{1 - e^{-2\lambda(l-u)}}{\frac{2}{Q} e^{-\lambda(l-u)} + (1 - \frac{1}{Q})(1 + e^{-2\lambda(l-u)})} \quad (1)$$

$$\Delta = \frac{\left[P(Q-1)u - \frac{\tau_f \psi u^2}{2}(Q-2) + \left(P - \tau_f \psi u\right) \frac{1 - e^{-\lambda(l-u)}}{1 + e^{-\lambda(l-u)}} \frac{Q-2}{\lambda} - \tau_f \psi l \right]}{A_m E_m} \quad (2)$$

Where, τ_{max} is the maximum elastic bond strength at the fibre-matrix interface; τ_f is the frictional bond stress at the fibre-matrix interface; u is the debonded length of fibre; ψ is the fibre perimeter;

$$Q = \frac{(A_m E_m + A_f E_f)}{A_m E_m} \quad (3)$$

and,

$$\lambda = \sqrt{\frac{\psi k}{A_m E_m} + \left[1 + \frac{A_m E_m}{A_f E_f}\right]} \quad (4)$$

in which A_m, A_f, E_m, and E_f are the matrix, fibre cross-sectional areas and elastic moduli respectively, and k is the interfacial bond modulus.

3.2. Full debonding stage

When $P \geq P_1$, the fibre is assumed to be complete debonding after the slip Δ_1, and no mechanical anchorage before the slip Δ_1 (Fig. 6). The pull-out load (P_1) can be predicted by the following equation [21,29].

$$P_1 = \psi \tau f_d(\Delta) \times (l - \Delta) \quad (5)$$

Where, (l-Δ) is the length of fibre remaining embedded for any slip Δ, and τ_{fd} (Δ) is the frictional shear stress for a slip Δ; the subscript "d" implies damage or decay. The frictional shear stress can be assumed constant for any slip Δ. However, as in real tests, it is shown to deteriorate with increasing slip, its value as derived in Naaman et al. [18,21,29] is given by:

$$\tau_{fd}(\Delta) = \tau_{fi}\frac{e^{-(\Delta-\Delta_0)^{\eta}-\xi e^{-(l)^{\eta}}}}{1-\xi e^{-(l-\Delta+\Delta_0)^{\eta}}} \times \frac{1-EXP\left[\frac{-2\upsilon_f\mu(l-\Delta+\Delta_0)}{E_f r_f\left(\frac{1+\upsilon_m}{E_m}\right)+\left(\frac{1-\upsilon_f}{E_f}\right)}\right]}{1-EXP\left[\frac{-2\upsilon_f\mu l}{E_f r_f\left(\frac{1+\upsilon_m}{E_m}\right)+\left(\frac{1-\upsilon_f}{E_f}\right)}\right]} \quad (6)$$

Where Δ is the relative slip of the fibre after full debonding; Δ_0 is the relative slip of the fibre at end of full debonding; as a first approximation it can be taken equal to the slip at maximum load; ξ is the damage coefficient, a dimensionless constant to give the analytical descending branch of the bond shear stress versus slip curve the same decaying trend as the experimental one; μ is the friction coefficient of the fibre-matrix interface; v is the Poisson's ratio, with subscript "f" for fibre and "m" for matrix; and η is the coefficient describing the exponential shape of the descending branch of the bond shear stress versus slip curve; for smooth steel fibres, a value of 0.2 is recommended by Naaman et al. [21,29].

3.3. Mechanical anchorage stage

Once complete debonding has occurred at the fibre-matrix interface, the horizontal portion of the fibre would still be subjected to interfacial frictional stresses and the hooked end of the fibre undergoes cold work deformation through two plastic hinges as indicated in Fig. 5b. The corresponding increase in the pull-out load value, due to the cold work from both plastic hinges, would then be added to P_1, resulting in a plateau load (P_2). This plateau value remains until the fibre is pulled by an additional distance "L_2", after which there would be only one active plastic hinge in the hooked end (Fig. 5c), and the pull-out load would drop to P_3. The new load at P_3 would then be held constant as the fibre is pulled-out by an additional distance "L_1" after which the pull-out load versus fibre end displacement can then be described using the frictional pull-out model of straight fibres developed by Naaman et al. [21] (Fig. 5d).

The first plateau load at P_2 (Fig. 6) due to the contribution of two plastic hinges can be estimated by:

$$P_2 = P_1 + \Delta P' \quad (7)$$

Where P_1 = Pull-out load at onset of complete debonding and $\Delta P'$ = Pull-out load due to two plastic hinges.

Similarly, the second pull-out load plateau at P_3 (Fig. 6) can be defined as:

$$P_3 = P_1 + \Delta P'' \quad (8)$$

Where, $\Delta P''$ = Pull-out load due to one plastic hinge.

In order to determine the value of $\Delta P'$ and $\Delta P''$, Alwan et al. [18] developed an equivalent pulley model (Fig. 7). The model simply consists of two frictional pulleys. Both Pulleys have rotational and tangential components of friction resisting the pull-out process. The rotational friction component correspond to the cold work needed for straightening the steel fibre at the plastic hinge location, and is represented by F_{PH} in Fig.7. The tangential friction component represents the work of Coulomb friction between the steel fibre and the matrix at the contact corner during the straightening of the fibre; it is represented by F_1 and F_2 in Fig. 7. T_1 and T_2 represent the chord tension before and after the first pulley respectively.

$$T_1 = \Delta P' \quad (9)$$

and that,

$$T_2 = \Delta P'' \quad (10)$$

R_1 and R_2 in Fig. 7 represent the reaction forces at the pulley centres; they are directly related to F_1 and F_2 through the kinetic coefficient of friction between the fibre and the matrix, μ. From equilibrium in the Fig. 7, the following relation can be derived:

$$T_1 = 2F_{PH} + F_1 + F_2 \quad (11)$$

$$T_2 = F_{PH} + F_2 \quad (12)$$

Where,

$$F_1 = R_1 \times \mu \quad (13)$$

And,

$$F_2 = R_2 \times \mu \quad (14)$$

But,

$$R_1 = T_1 \times cos\beta + T_2 * cos\beta \quad (15)$$

And,

$$R_2 = T_2 \times cos\beta \quad (16)$$

Hence,

$$T_1 = \frac{2F_{PH}\left[1 + \frac{\mu \times cos\beta}{1 - \mu \times cos\beta}\right]}{1 - \mu \times cos\beta} \quad (17)$$

$$T_2 = \frac{F_{PH}}{1 - \mu \times cos\beta} \quad (18)$$

The values of F_{PH} was determined from the equilibrium of moments about points from the equilibrium of moments about point "A" in the free body diagram sketch of the fibre plastic hinge presented in Fig. 8.

$\sum M_A = 0$

Thus,

$$M_P = F_{PH} \times (Moment\ arm = d_f * cos\theta) \quad (19)$$

Or,

$$F_{PH} = \frac{M_P}{d_f \times cos\theta} \quad (20)$$

The plastic moment of the steel fibre circular section, estimated as:

$$M_P = [f_y \times \frac{\pi r_f^2}{2} \times \frac{d_f}{3}] \quad (21)$$

Where, r_f, d_f = the fibre radius and diameter, respectively and σ_y = the fibre yield strength

By substituting (20) in (17), we get:

$$\Delta P' = T_1 = \frac{\frac{\sigma_y \times \pi r_f^2}{3 \times cos\theta}\left[1 + \frac{\mu \times cos\beta}{1 - \mu \times cos\beta}\right]}{1 - \mu \times cos\beta} \quad (22)$$

Also by substituting (20) in (18), we get:

$$\Delta P'' = T_2 = \frac{\frac{\sigma_y \times \pi r_f^2}{6 \times cos\theta}}{1 - \mu \times cos\beta} \quad (23)$$

4. Proposed model for pull-out behaviour of 4DH and 5DH fibres

Based on the analytical procedure of the 3DH fibre illustrated above, an extended model is proposed to account for the mechanical contribution provided by the hook of 4DH and 5DH fibres. From Fig. 1, it can be seen that the shape of the hook is idealized as three and four discrete hinges for 4DH and 5DH fibres respectively. Figs. 9 and 10 show the pull-out process of 4DH and 5DH fibres, according to the three pull-out stages specified for 3DH fibres. It can be observed that the pull-out process of these fibres basically consist of five (4DH) and six (5DH) stages.

The four stages of the 3DH fibre pull-out scenario apply to 4DH and 5DH fibres as well (Figs. 9 and 10); however, the mechanical anchorage stage (Figs. 5b and c) is extended due to the plastic deformation contribution of three and four hinges (Figs. 11a and b, respectively). In order to determine the values of pull-out load due to three and four plastic hinges; an equivalent pulley model is also extended, as described below:

4.1. Three hinges (4DH)

From equilibrium (Fig. 12a), the following can be stated:

$$T_1 = 3F_{PH} + F_1 + F_2 + F_3 \quad (24)$$

Moreover,

$$F_1 = R_1 * \mu \quad (25)$$

$$F_2 = R_2 * \mu \quad (26)$$

$$F_3 = R_3 * \mu \quad (27)$$

but,

$$R_1 = T_1 * cos\beta + T_2 * cos\beta \quad (28)$$

$$R_2 = T_2 * cos\beta + T_3 * cos\beta \quad (29)$$

$$R_3 = T_3 * cos\beta \quad (30)$$

Substituting (*25*)-(*27*) in (*24*), we get:

$$\therefore T_1 = \frac{F_{PH}\left[3+\left(\frac{2\mu*cos\beta}{1-\mu*cos\beta}\right)\left[2\left(1+\frac{\mu*cos\beta}{1-\mu*cos\beta}\right)+1\right]\right]}{(1-\mu*cos\beta)} \quad (31)$$

4.2. Four hinges (5DH)

From equilibrium (Fig. 12b), the following can be stated:

$$T_1 = 4F_{PH} + F_1 + F_2 + F_3 + F_4 \quad (32)$$

moreover,

$$F_1 = R_1 * \mu \quad (33)$$

$$F_2 = R_2 * \mu \quad (34)$$

$$F_3 = R_3 * \mu \quad (35)$$

$$F_4 = R_4 * \mu \quad (36)$$

but,

$$R_1 = T_1 * cos\beta + T_2 * cos\beta \quad (37)$$

$$R_2 = T_2 * cos\beta + T_3 * cos\beta \quad (38)$$

$$R_3 = T_3 * cos\beta + T_4 * cos\beta \quad (39)$$

$$R_4 = T_4 * cos\beta \quad (40)$$

substituting (*33*)-(*36*) in (*32*), we get:

$$\therefore T_1 = \frac{F_{PH}\left[4+\left(\frac{2\mu*cos\beta}{1-\mu*cos\beta}\right)\left[3+2\mu*cos\beta\left[2\left(1+\frac{\mu*cos\beta}{1-\mu*cos\beta}\right)+1\right]+2\left(1+\frac{\mu*cos\beta}{1-\mu*cos\beta}\right)+1\right]\right]}{(1-\mu*cos\beta)}$$

By using the above described procedure for 3DH fibre, the pull-out load (P) as a function of fibre slip (Δ) in all stages for 4DH (Eq. (42)) and 5DH (Eq. (43)) fibres can be obtained as follows:

$$P=\begin{cases} P_1\ (Eq.3) & \Delta_1 \\ \Delta P' = T_1\ (Eq.A8) \rightarrow P_2 = P_1 + \Delta P' & \Delta_2 = \Delta_1 + u \\ \Delta P'' = T_2\ (Eq.22) \rightarrow P_3 = P_1 + \Delta P'' & \Delta_3 = \Delta_2 + L_3 \\ \Delta P''' = T_3\ (Eq.23) \rightarrow P_4 = P_1 + \Delta P''' & \Delta_4 = \Delta_3 + L_2 \\ P_5 & \Delta_5 = \Delta_4 + L_1 \end{cases} \quad (42)$$

$$P=\begin{cases} P_1\ (Eq.3) & \Delta_1 \\ \Delta P' = T_1\ (Eq.A18) \rightarrow P_2 = P_1 + \Delta P' & \Delta_2 = \Delta_1 + u \\ \Delta P'' = T_2\ (Eq.A8) \rightarrow P_3 = P_1 + \Delta P'' & \Delta_3 = \Delta_2 + L_4 \\ \Delta P''' = T_3\ (Eq.22) \rightarrow P_4 = P_1 + \Delta P''' & \Delta_4 = \Delta_3 + L_3 \\ \Delta P'''' = T_4\ (Eq.23) \rightarrow P_5 = P_1 + \Delta P'''' & \Delta_5 = \Delta_4 + L_2 \\ P_6 & \Delta_6 = \Delta_5 + L_1 \end{cases} \quad (43)$$

The plastic moment formula is proposed as Eq. (44) to match the full plastic deformation for this fibre/matrix combination (Fig. 13).

$$M_P = F_h \times \frac{8r}{3\pi} = (\sigma_y \times \frac{\pi r^2}{2}) \times \frac{8r}{3\pi}$$

So,

$$M_P = \frac{4\sigma_y r_f^3}{3} \quad (44)$$

Where, $\frac{8r}{3\pi}$ is the true distance between centroids for the tension and compressive forces, F_h.

It should be noted that the previous formula for plastic moment (Eq. 21) was estimated in the Alwan et al. [18] model. Their approximation appears not to represent the plastic moment of the steel fibre circular as accurately. It is assumed that a fully deformed fibre is essential to pull-out without damage occurring to the UHPM matrix. In a weaker concrete an elastic-plastic deformation condition is sufficient for pull-out to occur [18,25]. Further work is proposed to understand the behaviour of each fibre geometry for this condition. This paper assumes that moderate hook angles (Table 2) require straightening under a moment given by Eq.(44).

To ascertain the reliability of the proposed formula for the plastic moment, the predicted pull-out curves are also compared with that adopted by Alwan et al. [18]. It can be seen here that their predictions underestimates the mechanical anchorage contribution (Table 3). However, the deviations shown in Table 3 do not exceed 11%. On the other hand, the proposed model is also compared with Zile model [25] for single hooked end fibre (i.e. 3DH). Zile's model [25] appears to underestimate the mechanical anchorage contribution by a greater amount than Alwan's model (Fig. 14). This can be explained by the fact that Alwan's formula and Zile's model may not take into account the case of full deformation and straightening of the hook, which results in lower values of mechanical anchorage contribution. In both of these cited papers a normal strength matrix applies.

5. Model validation

5.1. Comparison of experimental and modelling pull-out forces.

In order to ascertain the suitability of the proposed analytical model, comparisons are made between the experimental and predicted pull-out force curves as shown in Figs. 14-17. Fig. 14 applies to straight fibres (i.e. 3DS, 4DS and 5DS) and Figs. 14-16 apply to 3DH, 4DH and 5DH hooked end fibres. The input parameters used in this model are directly related to material properties of the fibre (i.e. fibre geometry and tensile strength

in Table 2). The results show that the proposed analytical model is able to predict the pull-out forces for all 3DH, 4DH and 5DH fibres.

5.2. Prediction of pull-out process

In addition to obtaining the pull-out load at all main pull-out stages, it is of interest to estimate the pull-out force across the whole duration of the test. Therefore, the predicted pull-out curves were fitted numerically using fifth degree polynomial function Eq. (45).

$$y = a_0 + a_1 x + a_2 x^2 + a_3 x^3 + a_4 x^4 + a_5 x^5 \quad (45)$$

To provide a more realistic transition between points (i.e. P_1, P_2…..P_5) based upon the present proposal, the coefficients data (a_0, a_1…… a_5) were provided by using MATLAB (see Table 4).

Figs. 15-17 show the comparison plots between model predictions and experimentally measured pull-out curves for 3DH, 4DH and 5DH fibres. All curves show that the proposed model is able to take into account the mechanical anchorage effect provided by the fibre hook. The results also show that the model is able to capture the main features of pull-out behaviour and to predict accurately the pull-out load-slip response, irrespectively of fibre geometry and tensile strength.

6. Conclusions

- A straightforward and comprehensive model is developed to simulate the mechanical anchorage contribution provided by the hook. It is assumed that the shape of the hook is idealized as the two, three and four plastic hinges for 3DH, 4DH and 5DH fibres, respectively. The mechanical contribution of the hook is a function of the cold work needed to straighten the fibre during the pull-out. The input parameters of the model are mainly the mechanical and geometrical properties of the fibres. Since the cementitious matrix is ultra-high performance mortar (UHPM), the damage of the matrix during the pull-out is neglected.
- Model predictions were compared against experimental results of pull-out tests. In order to ascertain the reliability of the proposed formula for plastic moment, pull-out curves are also compared with those obtained by Alwan's et al. [18] formula.

The results showed that the proposed model was able to describe the main features of anchorage mechanisms and to accurately predict the pull-out load-slip response. The present model takes into account the variation of the geometrical and tensile plastic flow properties as well as the rupture condition of the fibres. An ongoing study is currently being conducted to enlarge the scope of application of the present model to different matrix strengths (i.e. normal, medium, high strength matrixes). This is to include factors that were not covered in this paper (e.g. matrix damage and partial deformation when straightening the fibre hook).

Acknowledgments

The first author gratefully acknowledges the financial support of the Ministry of Higher Education and Scientific Research of Iraqi Government for this Ph.D. project.

Appendix A. Nomenclature

Nomenclature

P	pull-out force	k	interfacial bond modulus
ΔP	pull-out force due to plastic hinges contribution	ξ	damage coefficient
T	chord tension in the pulley	u	debonded length of fibre
F	tangential friction component	ν_f	poisson's ratio for fibre
F_{PH}	rotational friction component	ν_m	poisson's ratio for matrix
R	reaction forces at the pulley centres	V_f	fibre volume friction
Δ	relative slip of the fibre after full debonding	l	embedded length of fibre
Δ_0	relative slip of the fibre at end of full debonding	θ_1,θ_2,β	hook angles
τ_{max}	bond strength of interface between fibre-matrix	L	hook length
τ_f	frictional bond stress at the fibre-matrix interface	ψ	fibre perimeter
τ_{fd}	frictional shear stress	r_f	fibre radius
A_m	matrix cross-sectional area	d_f	fibre diameter
A_f	fibre cross-sectional area	σ_y	fibre yield strength
E_m	modulus of elasticity of matrix	σ_u	fibre ultimate strength
E_f	modulus of elasticity of fibre	M_P	plastic moment
μ	friction coefficient of the fibre-matrix interface		
η	factor reflective of steepness of descending branch of pull-out curve		

References

[1] Alberti M, Enfedaque A, Galvez J, Canovas M, Osorio I. Polyolefin fiber-reinforced concrete enhanced with steel-hooked fibers in low proportions. Mater Des 2014;60:57-65.

[2] Kaïkea A, Achoura D, Duplan F, Rizzuti L. Effect of mineral admixtures and steel fiber volume contents on the behavior of high performance fiber reinforced concrete. Mater Des 2014;63:493-9.

[3] Holschemacher K, Mueller T, Ribakov Y. Effect of steel fibres on mechanical properties of high-strength concrete. Mater Des 2010;31:2604-15.

[4] Nguyen T, Toumi A, Turatsinze A. Mechanical properties of steel fibre reinforced and rubberised cement-based mortars. Mater Des 2010;31:641-7.

[5] Zheng W, Li H, Wang Y. Compressive behaviour of hybrid fiber-reinforced reactive powder concrete after high temperature. Mater Des 2012;41:403-9.

[6] Rambo DAS, de Andrade Silva F, Toledo Filho RD. Mechanical behavior of hybrid steel-fiber self-consolidating concrete: materials and structural aspects. Mater Des 2014;54:32-42.

[7] Prakash A, Srinivasan S, Rao ARM. Numerical investigation on steel fibre reinforced cementitious composite panels subjected to high velocity impact loading. Mater Des 2015;83:164-75.

[8] Sanjayan JG, Nazari A, Pouraliakbar H. FEA modelling of fracture toughness of steel fibre-reinforced geopolymer composites. Mater Des 2015;76:215-22.

[9] Shah AA, Ribakov Y. Recent trends in steel fibered high-strength concrete. Mater Des 2011;32:4122-51.

[10] Won J, Hong B, Lee S, Choi SJ. Bonding properties of amorphous micro-steel fibre-reinforced cementitious composites. Composite Structures 2013;102:101-9.

[11] Won J, Lee J, Lee S. Bonding behaviour of arch-type steel fibres in a cementitious composite. Composite Structures 2015;133:117-23.

[12] Lee Y, Kang S, Kim J. Pullout behavior of inclined steel fiber in an ultra-high strength cementitious matrix. Constr Build Mater 2010;24:2030-41.

[13] Gray R. Experimental techniques for measuring fibre/matrix interfacial bond shear strength. Int J Adhes Adhes 1983;3:197-202.

[14] Robins P, Austin S, Jones P. Pull-out behaviour of hooked steel fibres. Mater Struct 2002;35:434-42.

[15] Prakash A, Srinivasan S, Rao ARM. Numerical investigation on steel fibre reinforced cementitious composite panels subjected to high velocity impact loading. Mater Des 2015;83:164-75.

[16] Abu-Lebdeh T, Hamoush S, Heard W, Zornig B. Effect of matrix strength on pullout behavior of steel fiber reinforced very-high strength concrete composites. Constr Build Mater 2011;25:39-46.

[17] Won J, Lee J, Lee S. Flexural behaviour of arch-type steel fibre reinforced cementitious composites. Composite Structures 2015;134:565-71.

[18] Alwan JM, Naaman AE, Guerrero P. Effect of mechanical clamping on the pull-out response of hooked steel fibers embedded in cementitious matrices. Concrete Science and Engineering 1999;1:15-25.

[19] Chanvillard G. Modeling the pullout of wire-drawn steel fibers. Cem Concr Res 1999;29:1027-37.

[20] Sujivorakul C. Development of high performance fiber reinforced cement composites using twisted polygonal steel fibers. : University of Michigan., 2002.

[21] Naaman AE, Namur GG, Alwan JM, Najm HS. Fiber pullout and bond slip. I: Analytical study. J Struct Eng 1991;117:2769-90.

[22] Laranjeira F, Molins C, Aguado A. Predicting the pullout response of inclined hooked steel fibers. Cem Concr Res 2010;40:1471-87.

[23] Ghoddousi P, Ahmadi R, Sharifi M. Fiber pullout model for aligned hooked-end steel fiber. Canadian Journal of Civil Engineering 2010;37:1179-88.

[24] Soetens T, Van Gysel A, Matthys S, Taerwe L. A semi-analytical model to predict the pull-out behaviour of inclined hooked-end steel fibres. Constr Build Mater 2013;43:253-65.

[25] Zīle E, Zīle O. Effect of the fiber geometry on the pullout response of mechanically deformed steel fibers. Cem Concr Res 2013;44:18-24.

[26] Won J, Lee J, Lee S. Predicting pull-out behaviour based on the bond mechanism of arch-type steel fibre in cementitious composite. Composite Structures 2015;134:633-44.

[27] Abdallah S, Fan M, Zhou X, Geyt S. Anchorage Effects of Various Steel Fibre Architectures for Concrete Reinforcement. International Journal of Concrete Structures and Materials 2016:1-11.

[28] Wille K, Naaman A. Bond stress-slip behavior of steel fibers embedded in ultra high performance concrete. 2010:99-111.

[29] Naaman AE, Namur GG, Alwan JM, Najm HS. Fiber pullout and bond slip. II: Experimental validation. J Struct Eng 1991;117:2791-800.

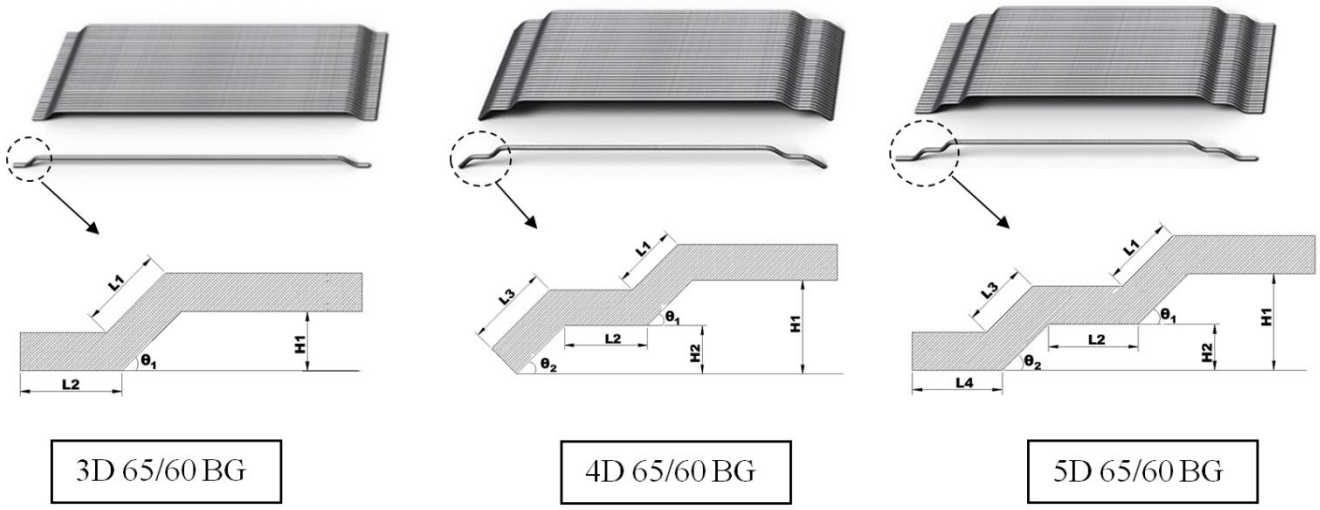

Fig. 1. Geometrical properties of hooked end steel fibres.

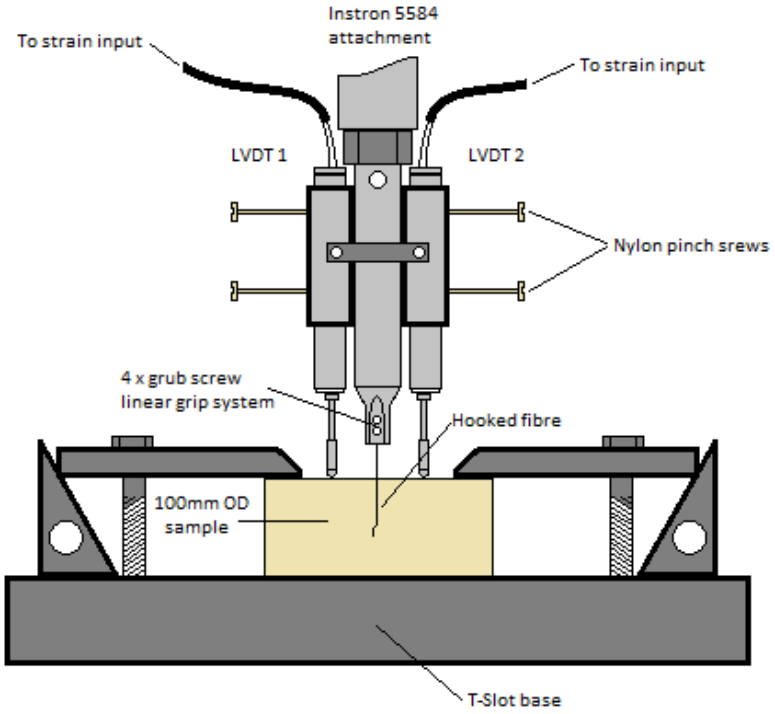

Fig. 2. Pull-out test setup.

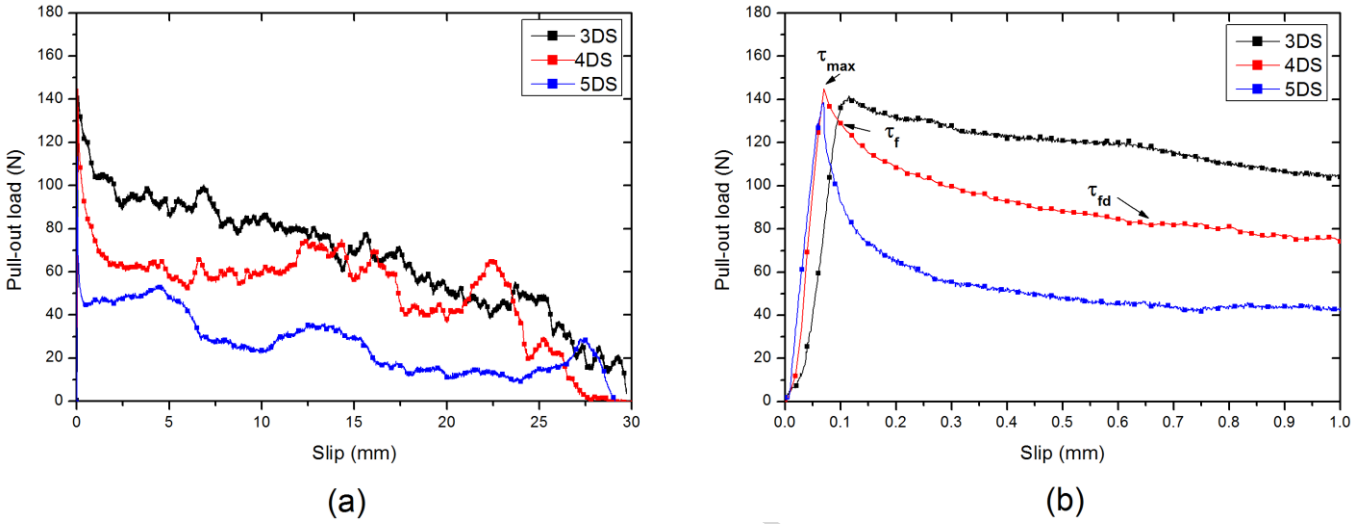

Fig. 3. Pull-out-slip response of straight steel fibres. (a) total pull-out curve and (b) detail up to a slip of 1mm.

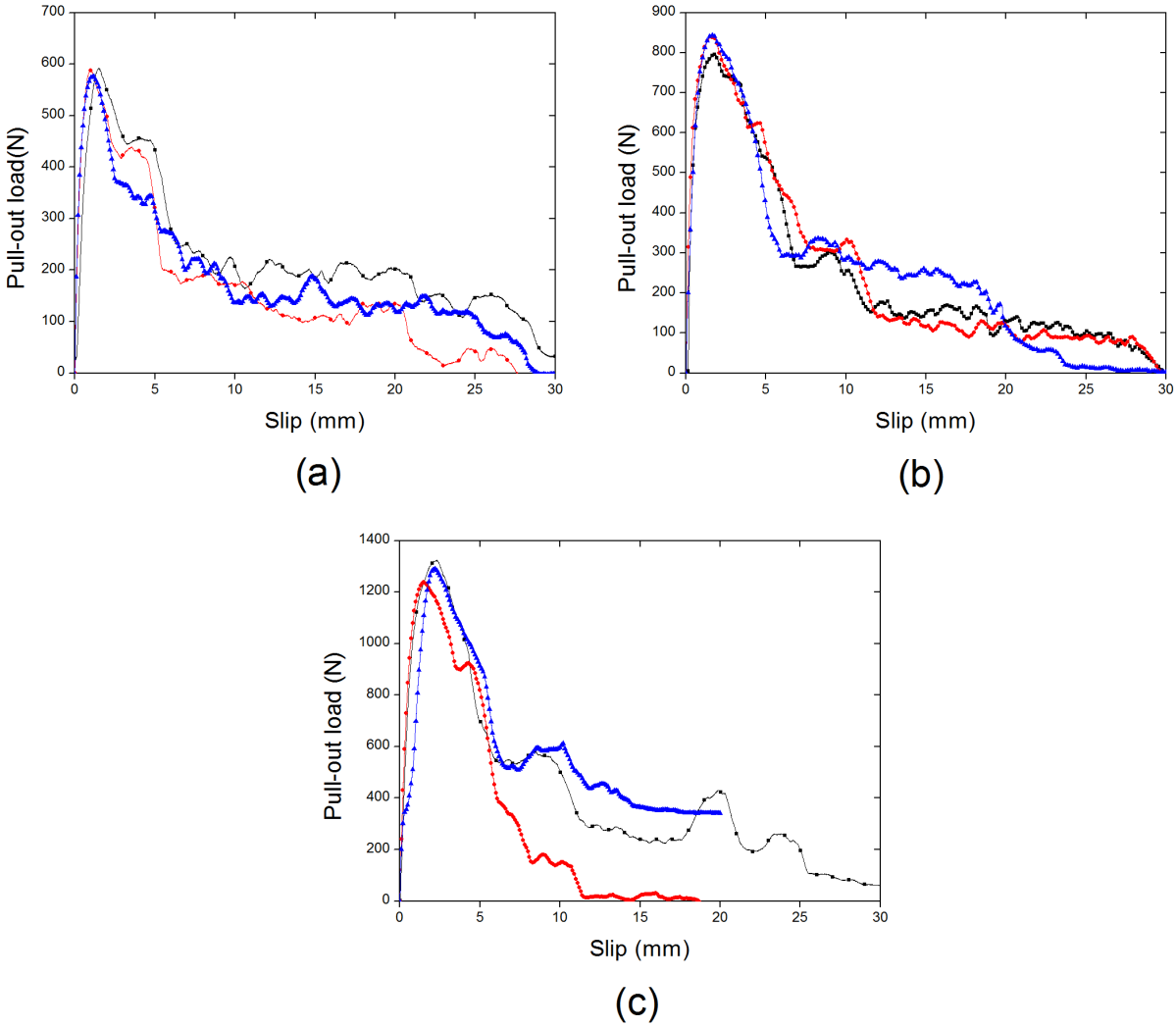

Fig. 4. Pull-out-slip response of hooked-end steel fibres. (a) 3DH, (b) 4DH and (c) 5DH fibres.

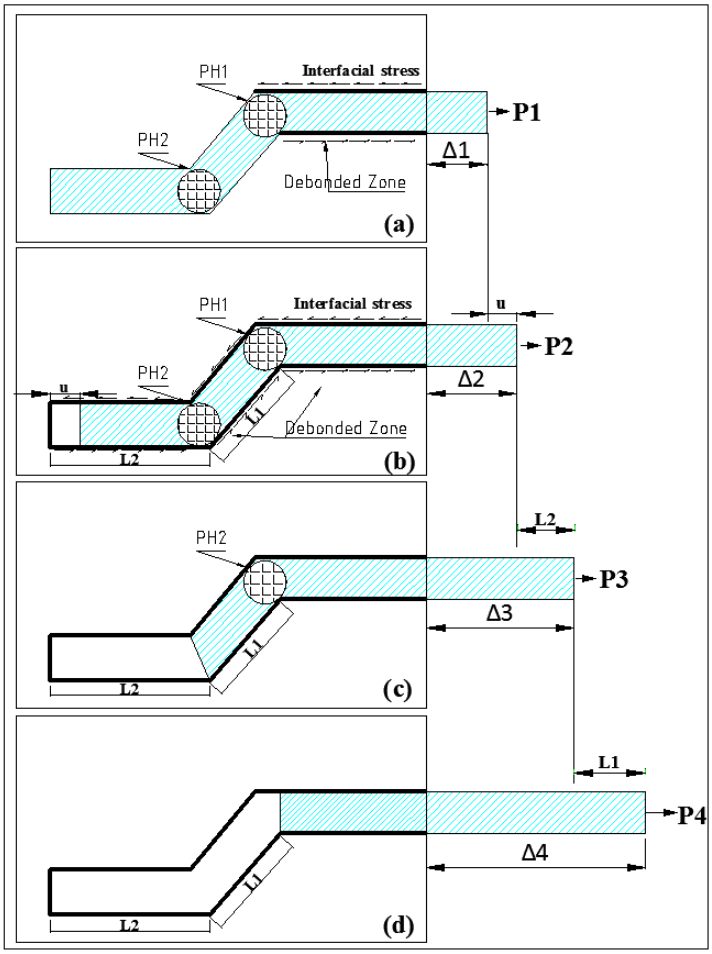

Fig. 5. a) Hooked-end steel fibre at onset of complete debonding, b) hooked steel fibre during mechanical interlock with two plastic hinges, c) mechanical interlock with one plastic hinge, and d) hooked steel fibre at onset of frictional pull-out [18].

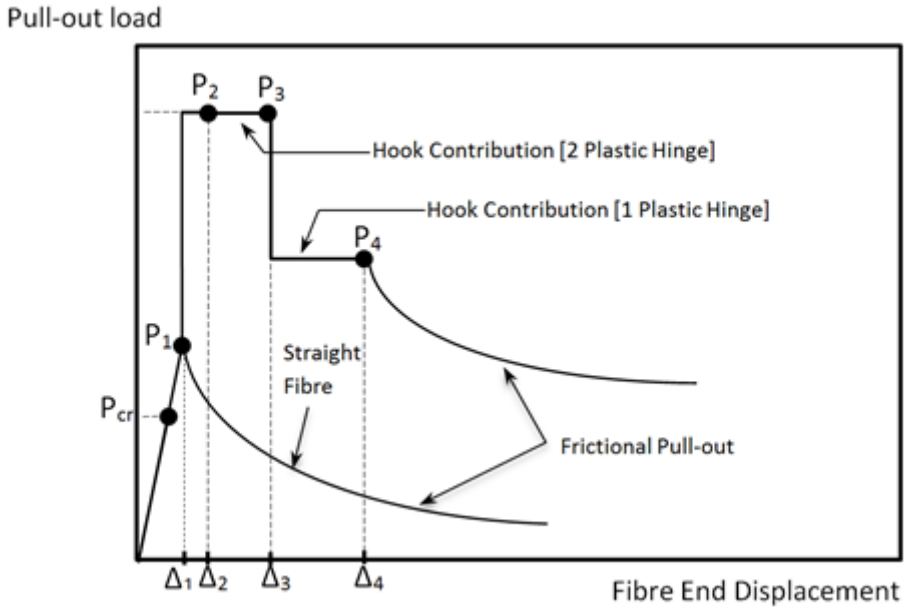

Fig. 6. Schematic sketch of the theoretical pull-out curve of a hooked steel fibre from a cementitious matrix [18].

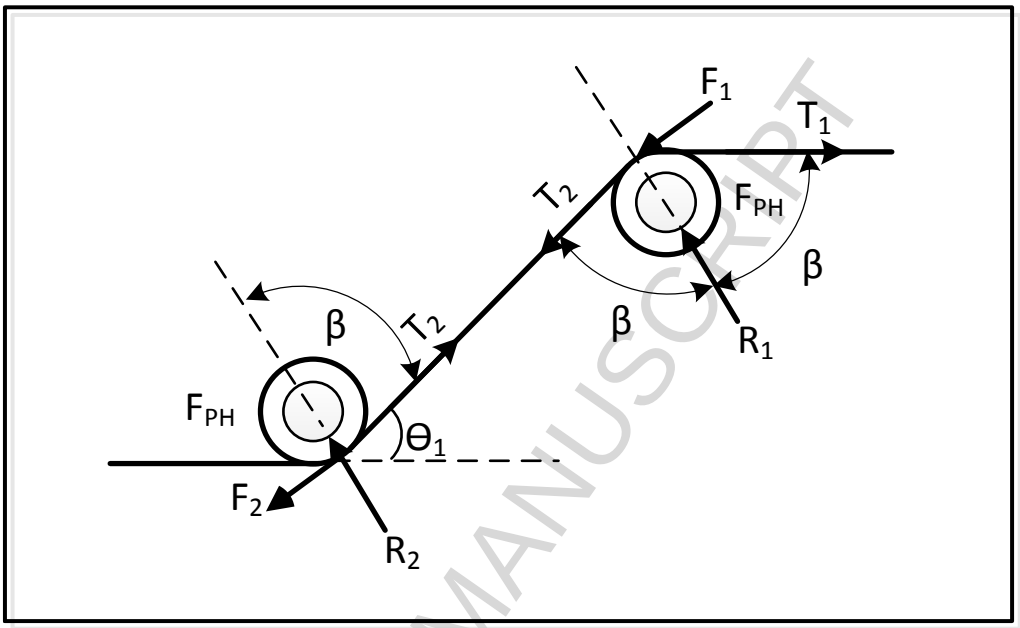

Fig. 7. Line sketch of the frictional pulley model of 3DH fibres [18].

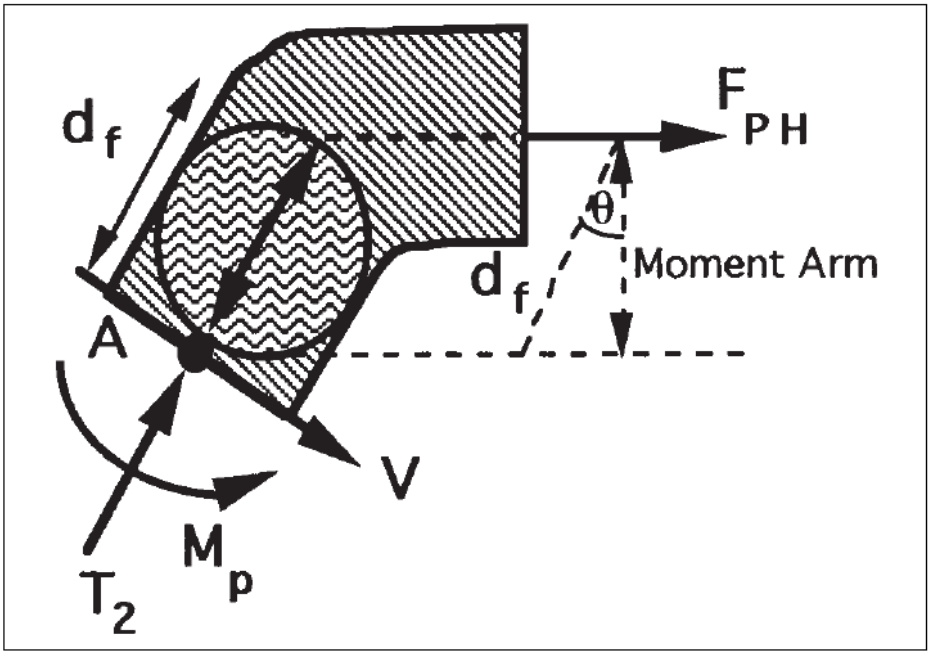

Fig. 8. Sketch of the free body diagram of the fibre plastic hinge [18].

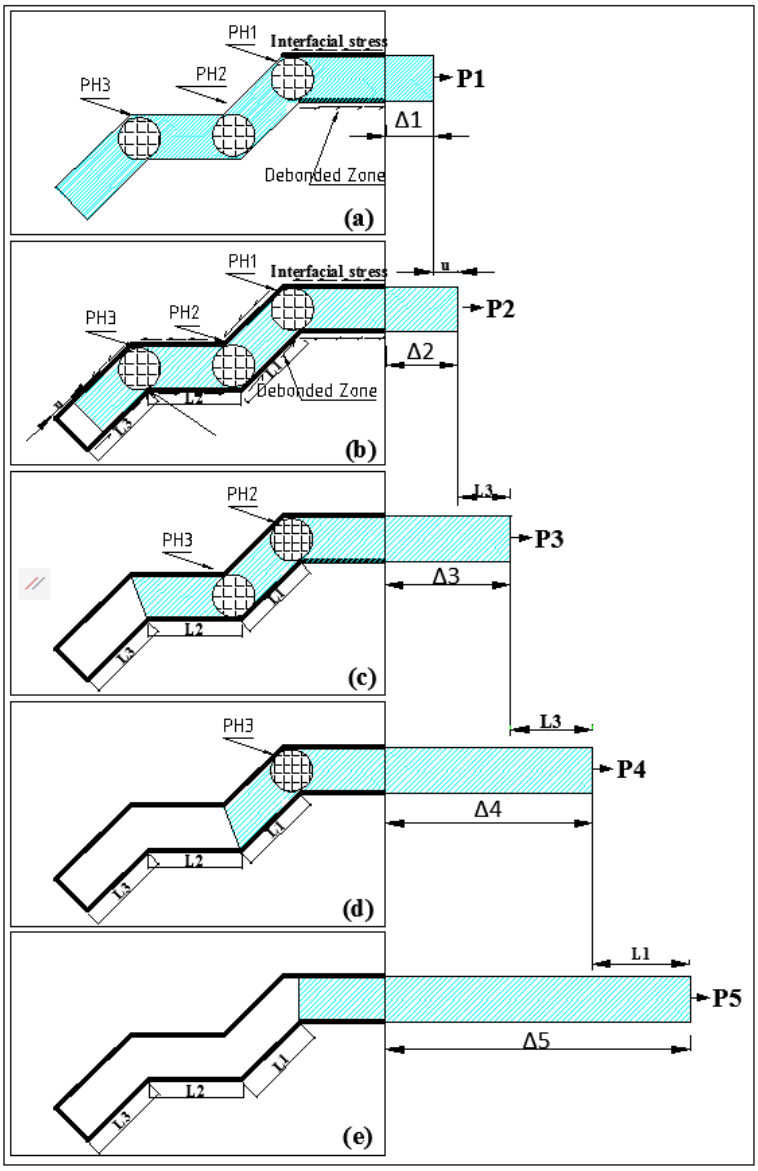

Fig. 9. a) Hooked-end steel fibre at onset of complete debonding, b) hooked steel fibre during mechanical interlock with three plastic hinges, c) mechanical interlock with two plastic hinge, d) mechanical interlock with one plastic hinge, and e) hooked steel fibre at onset of frictional pull-out.

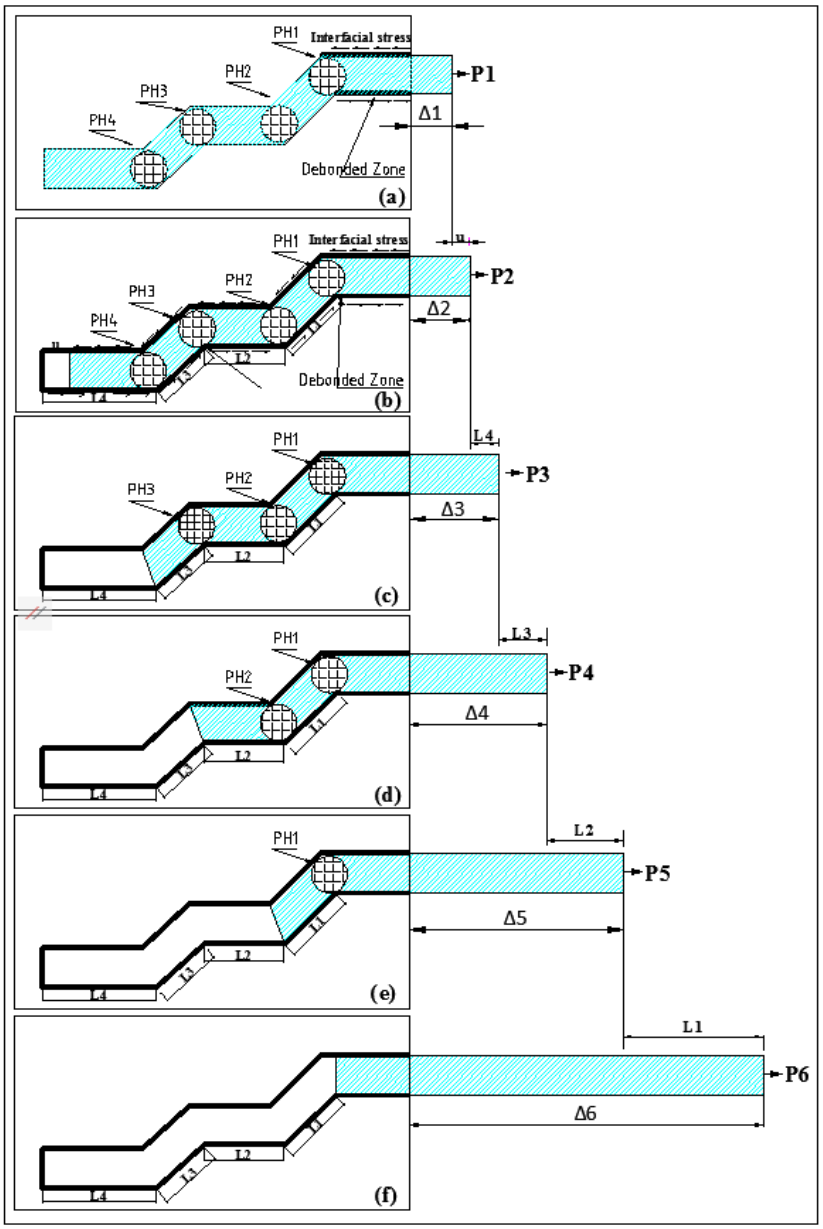

Fig. 10. a) Hooked-end steel fibre at onset of complete debonding, b) hooked steel fibre during mechanical interlock with four plastic hinges, c) mechanical interlock with three plastic hinge, d) mechanical interlock with two plastic hinge, e) mechanical interlock with one plastic hinge, and f) hooked steel fibre at onset of frictional pull-out.

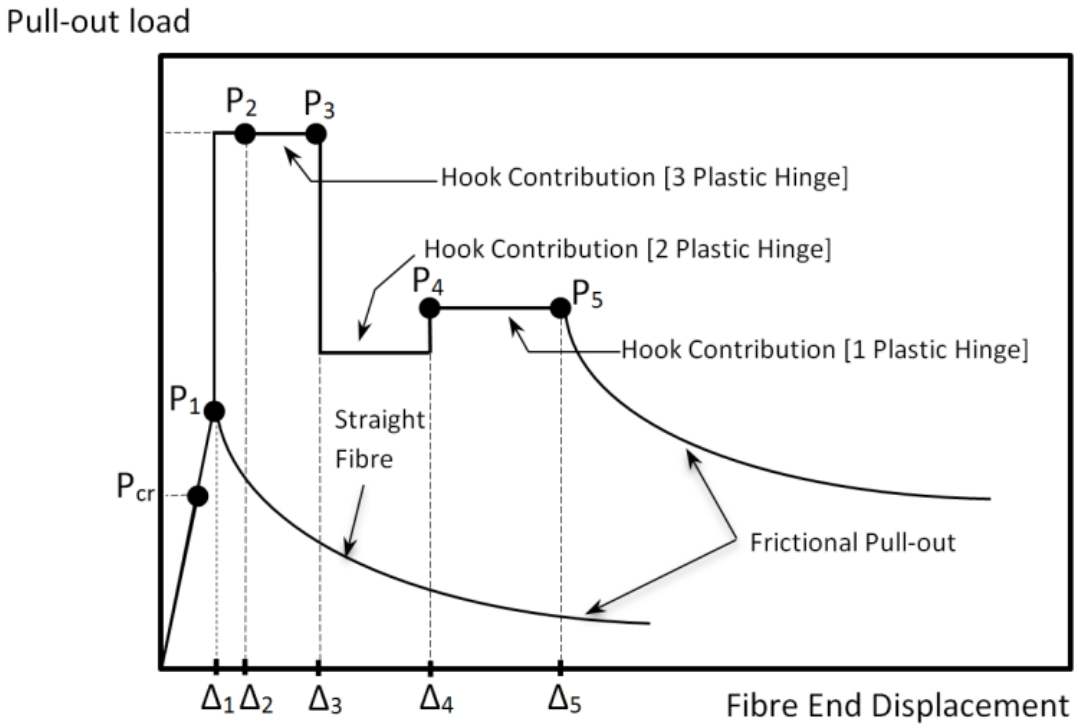

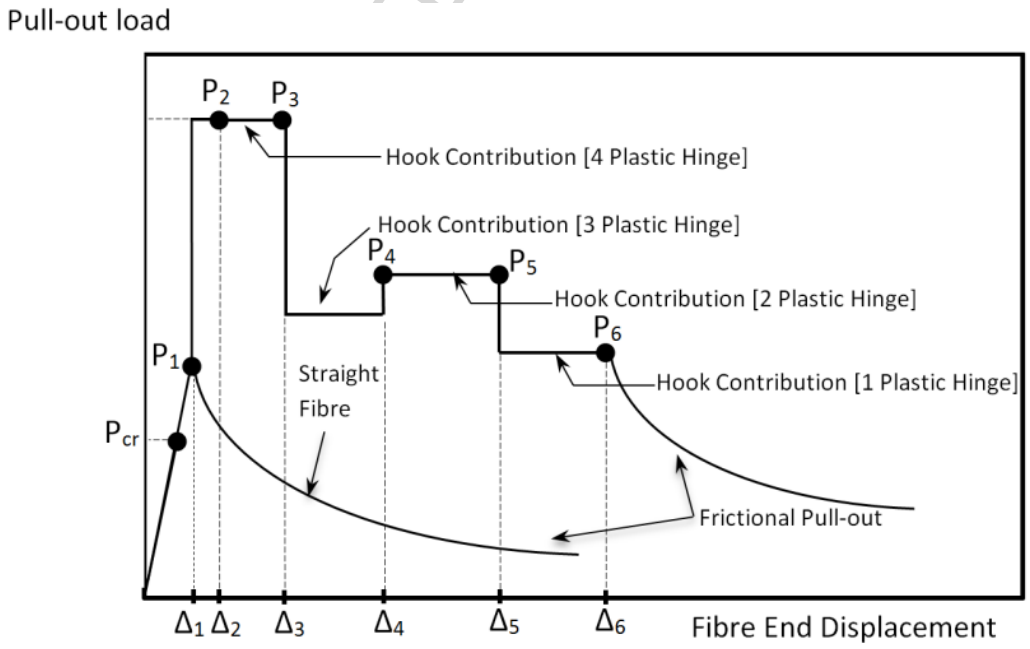

(b)

Fig. 11. Schematic sketch of the theoretical pull-out curve. (a) 4DH and (b) 5DH fibres.

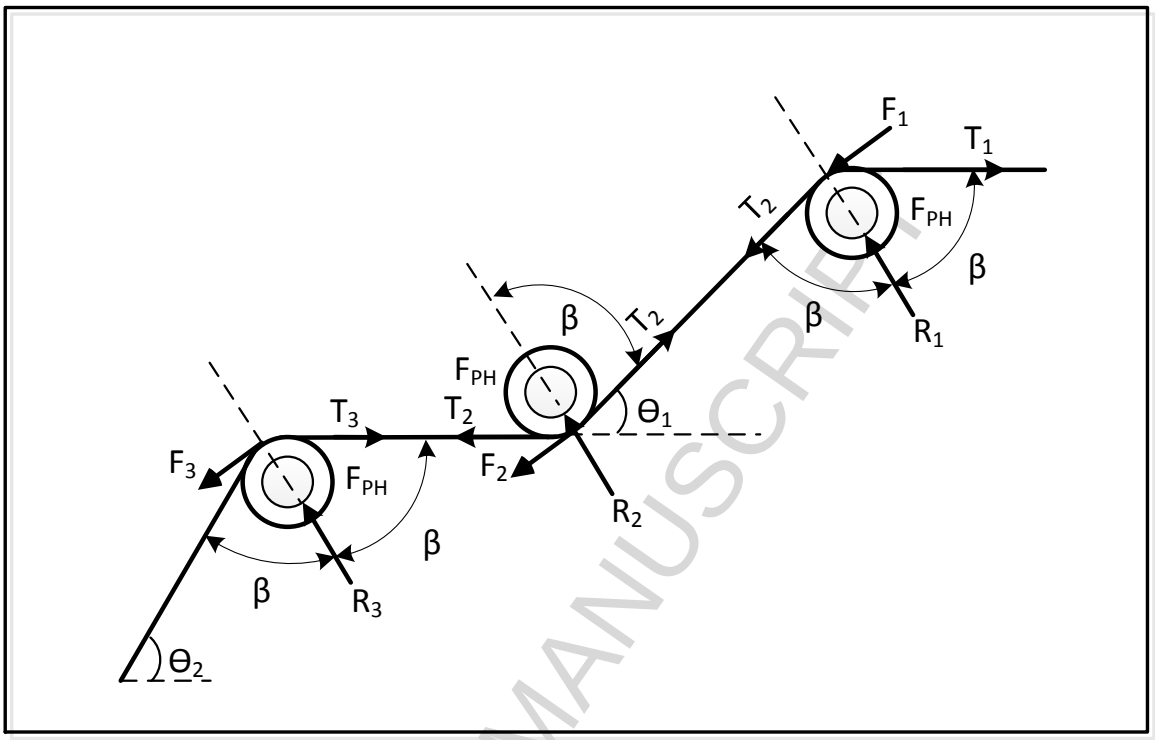

(a)

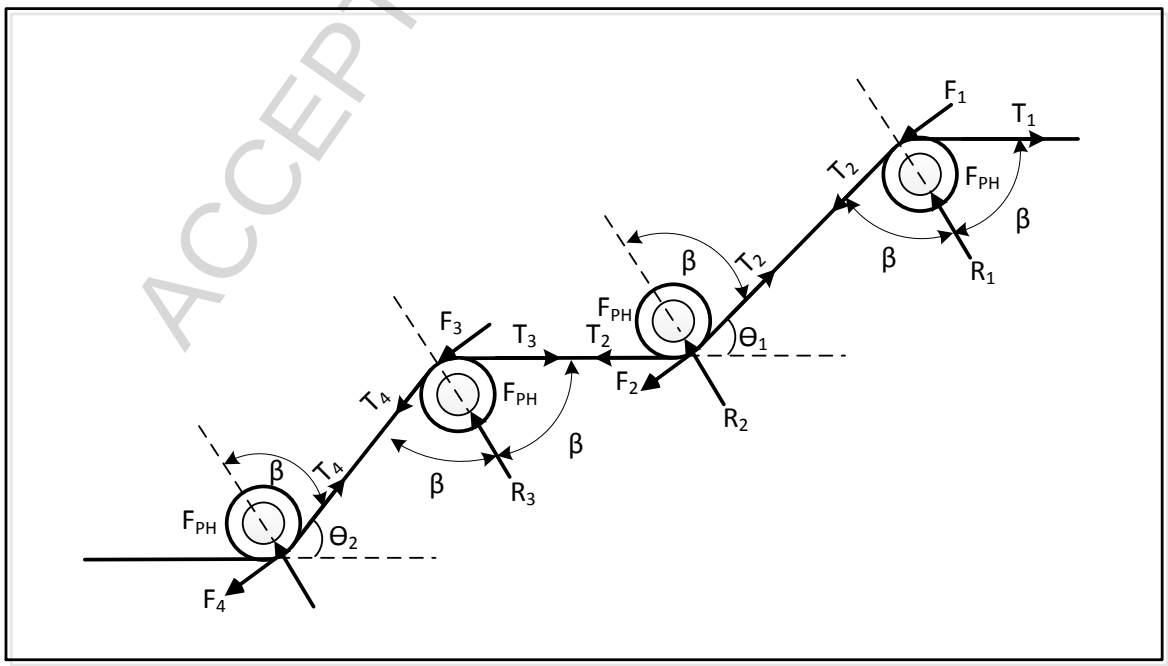

(b)

Fig. 12. Line sketch of the frictional pulley model. (a) 4DH and (b) 5DH fibres.

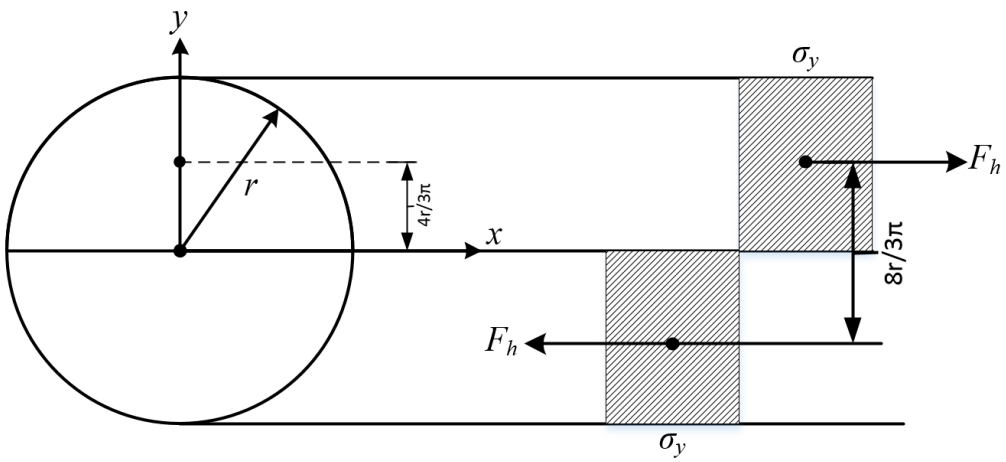

Fig. 13. Stress distribution of steel fibre circular section subjected to fully plastic deformation.

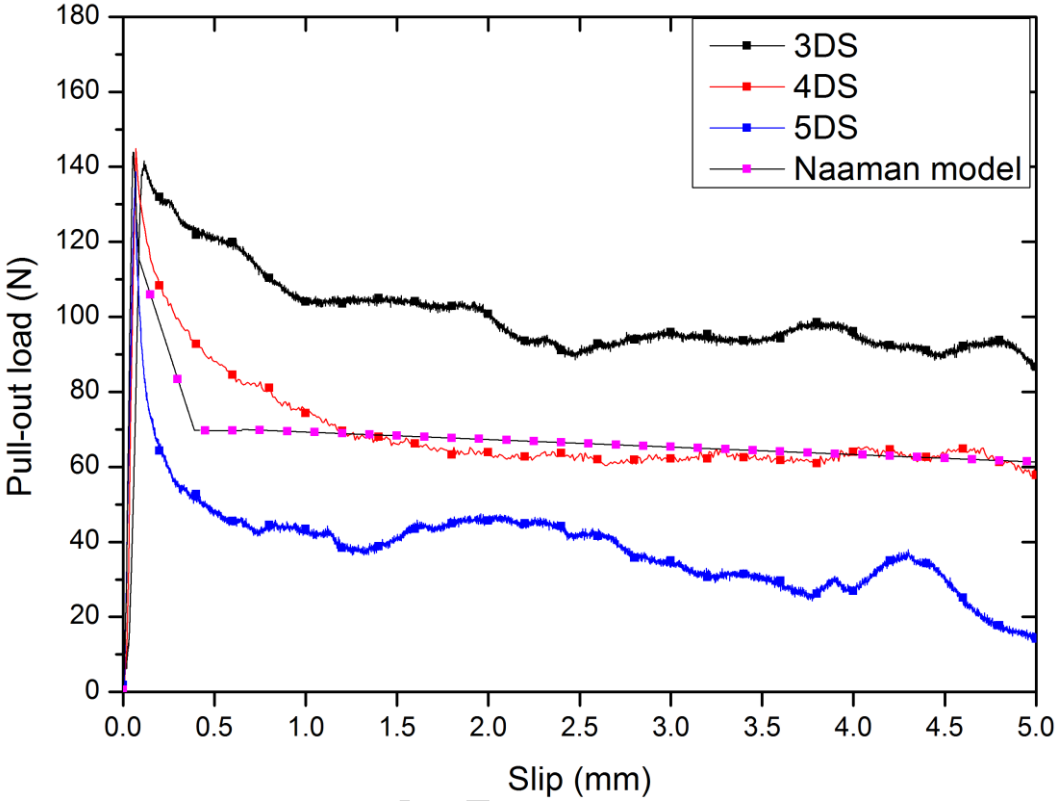

Fig. 14. Validation of the Naaman et al.[21] against experimental results for straight fibres.

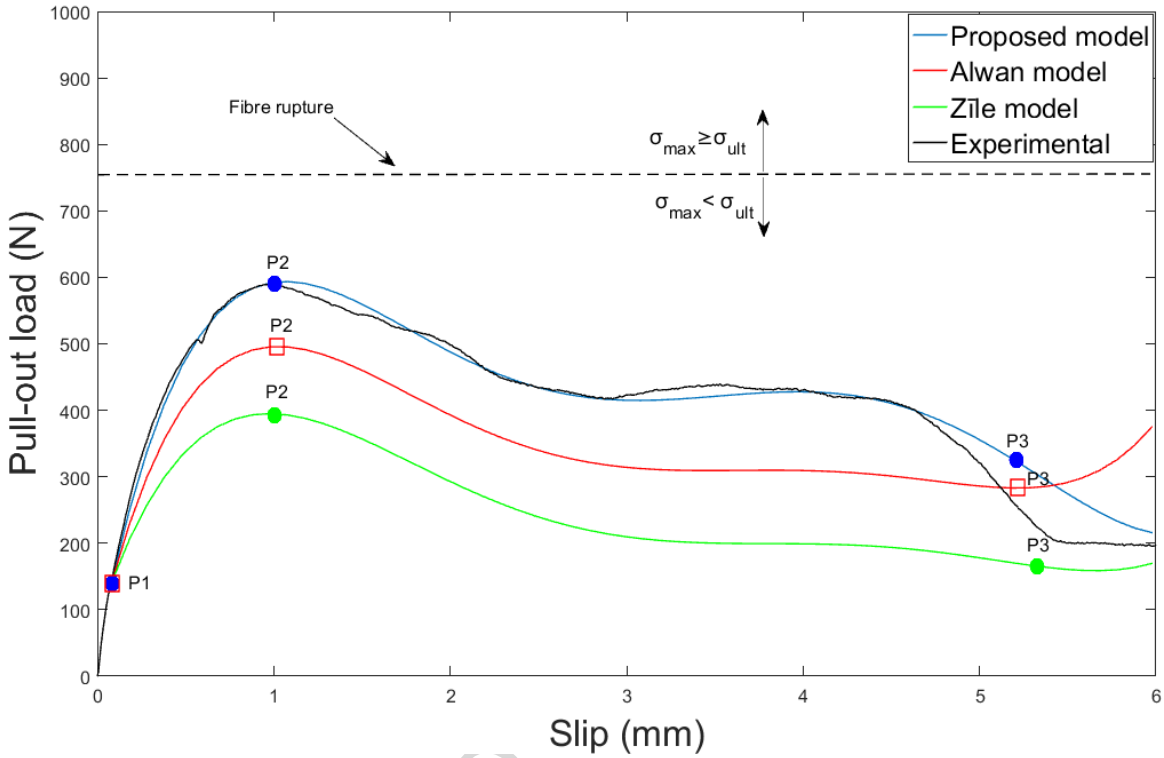

Fig. 15. Validation of the proposed model , Alwan et al.[18] model and Zile et al.[25] model against experimental results for 3DH fibres.

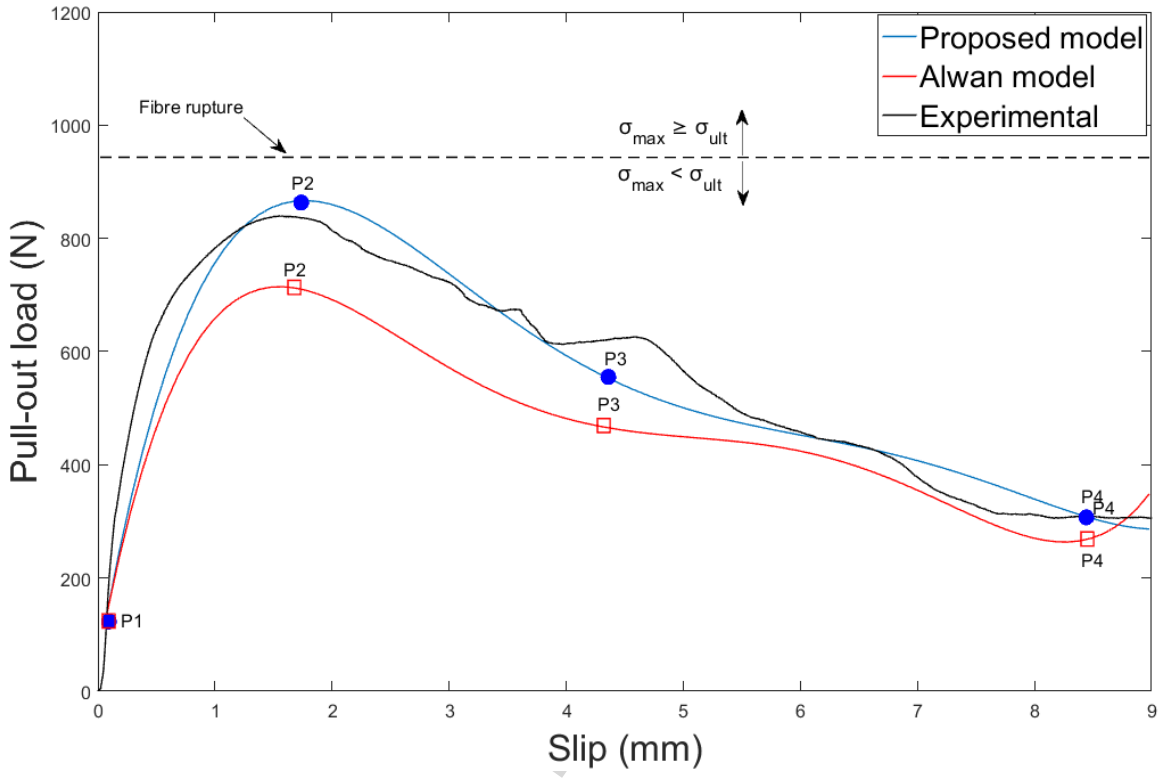

Fig. 16. Validation of the proposed model and Alwan et al.[18] model against experimental results of 4DH fibres.

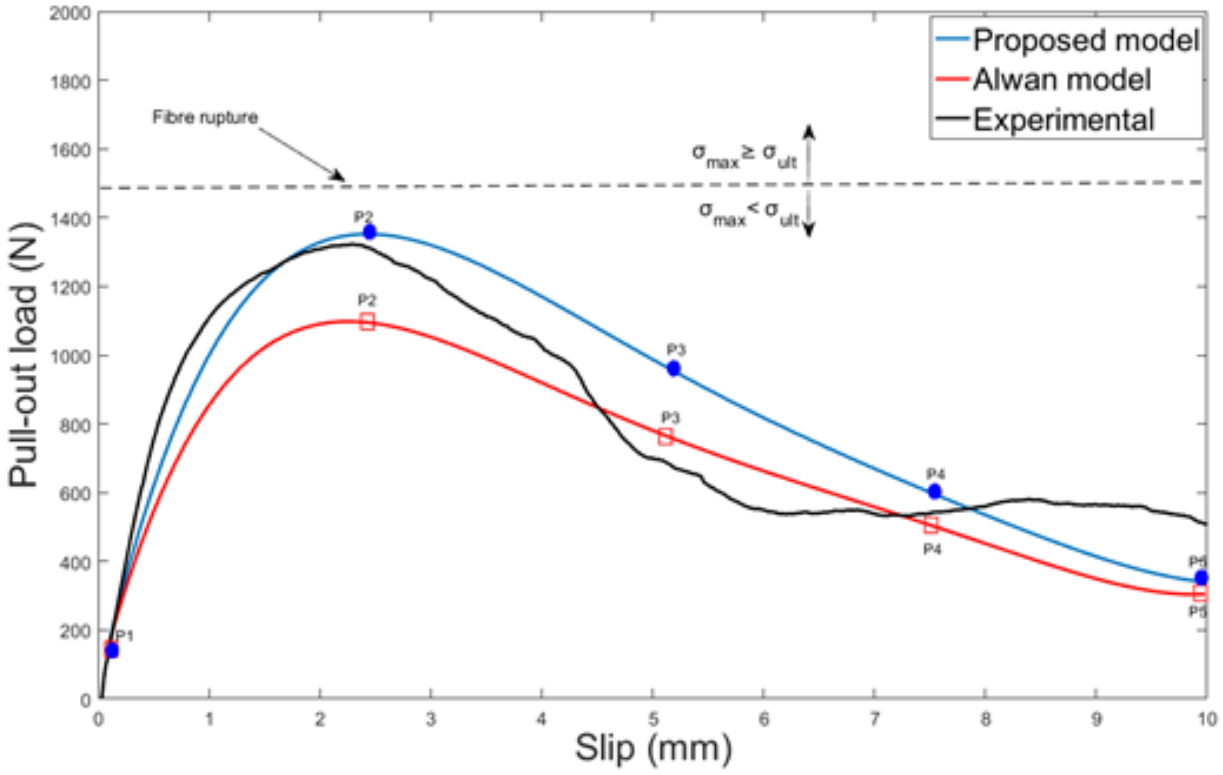

Fig. 17. Validation of the proposed model and Alwan et al.[18] model against experimental results of 5DH fibres.

Table 1

UHPM mixture compositions (values in kg/m^3)

Cement type III 52.2N	Silica fume	Ground quartz	Fine sand				
(150-600μm)	Superplasticizer	Accelerator	Water	f'_c*(MPa)*			
710	231	211	1020	31	30	230	152

Table 2

The measured geometric and mechanical properties of hooked-end fibres

Fibre type	σ_u* (MPa)	σ_y† (MPa)	l_f (mm)	d_f (mm)	Hook length (mm)				Hook angles (°)			Hook height (mm)	
					L1	*L2*	*L3*	*L4*	θ_1	θ_2	β	H1	H2
3D 65/60 BG	1150	775-985	60	0.90	2.12	2.95	-	-	45.7	45.5	67.5	1.85	-
4D 65/60 BG	1500	1020-1165	60	0.90	2.98	2.62	3.05	-	30.1	30.8	75.0	4.37	2.20
5D 65/60 BG	2300	1177-1455	60	0.90	2.57	2.38	2.57	2.56	27.9	28.2	76.0	2.96	1.57

* Ultimate strength
† Yield strength

Table 3

The obtained pull-out forces from the proposed model (Pm) and Alwan's model (Am)

Fibre type	P_1	CV	P_2	CV	P_3	CV	P_4	CV	P_5	CV					
	Pm	Am	(%)	Pm	Am	(%)	Pm	Am	(%)	Pm	Am	(%)	Pm	Am	(%)
3DH	140	140	0.0%	591	495	8.83	323	283	6.60	-	-	-	-	-	-
4DH	140	140	0.0%	867	710	9.95	561	469	8.93	323	283	6.60	-	-	-
5DH	140	140	0.0%	1353	1093	10.62	937	766	10.04	605	505	9.00	345	301	6.81

Table 4
Parameters of fifth degree polynomial function (see Eq. (27)).

Fibre type	a_0	a_1	a_2	a_3	a_4	a_5
3DH	38.79	3.43	-60.79	394	-1137	1354
4DH	48.23	0.40	-11.46	122.3	-596.1	1194
5DH	29.41	0.19	-6.52	84.96	-532.7	1424

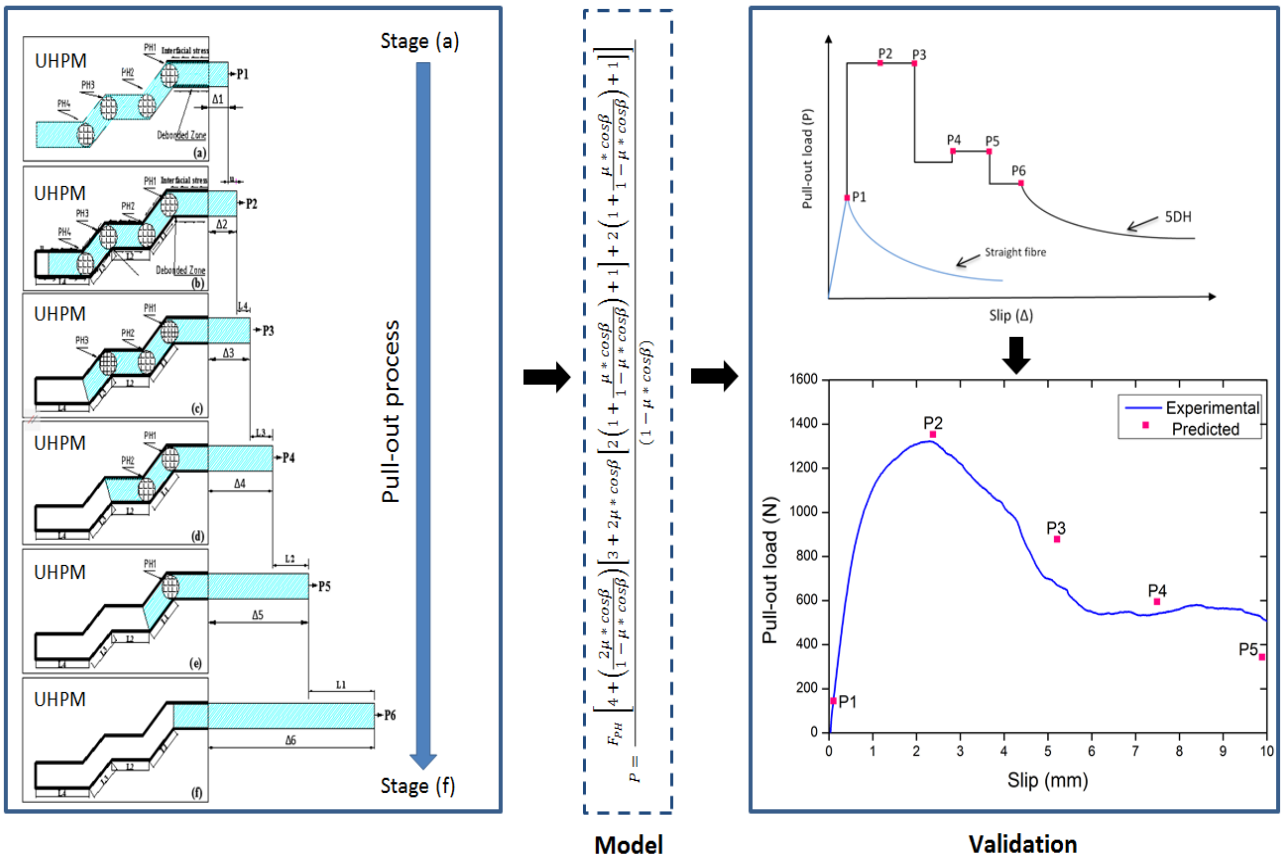

Graphical abstract

Highlights

The pull-out and straightening behaviour of various hooked end fibres in UHPM is determined and presented.

A simple model extended from the frictional pulley model is developed and mechanical anchorage effect simulated.

The model provides a good description of experimental pull-out results for the debonding and plastic straightening of the hook.